Soil Dynamics and Earthquake Engineering 161 (2022) 107387

Contents lists available at ScienceDirect

Soil Dynamics and Earthquake Engineering

journal homepage: www.elsevier.com/locate/soildyn

Robust estimation of 1D shear-wave quality factor profiles for site response analysis using seismic noise

Ilaria Dreossi [a,*], Stefano Parolai [b]

[a] National Institute of Oceanography and Applied Geophysics – OGS, Udine, Italy
[b] National Institute of Oceanography and Applied Geophysics – OGS, Sgonico, Italy

ARTICLE INFO

Keywords:
Simultaneous Algebraic Reconstruction Technique (SART)
Shear-wave quality factor (Q_S) inversion
Seismic attenuation
Site effects
Ambient seismic noise

ABSTRACT

Ambient seismic noise, particularly useful in urban areas, contains valuable information on seismic wave attenuation and the related shear-wave quality factor (Q_S) in the near-surface layers. Although the application of ambient seismic noise for attenuation studies is promising, more development and testing are necessary before it can be adopted for standard *in situ* analysis. In this paper, a development of the approach suggested in Parolai (2014) [58] is proposed and tested to improve the robustness of the results. In particular, the Simultaneous Algebraic Reconstruction Technique (SART) (Andersen and Kak, 1984) [5] is used for implementing an attenuation positivity constraint to the solutions – to non-get negative Q_S values – avoiding the preliminary testing of parameters required in the original procedure. Tests carried out at sites, where previous Q_S values estimated with the approach proposed by Parolai (2014) [58] were available, show similar results to the former algorithm. Furthermore, for the used data sets, the attenuation positivity constraint was shown not to be mandatory for gaining solutions with a physical meaning.

1. Introduction

The frequency-dependent changes in amplitude and duration of seismic waves while propagating in the uppermost portion of the crust, are caused by local morphological, geological, and geotechnical features, which together are generally defined as the site response. They are mainly determined by the impedance contrast between geological units. Although seismic amplification depends on several parameters [7], the shear-wave velocity (V_S) profile and the fundamental resonance frequency of a site are the most common proxies used for characterizing it in terms of site response. However, when a full characterization of the site response is required, detailed information on the mechanical characteristics of the material below a site must be added, including seismic attenuation. This is described by the quality factor Q, a quantity related to the relative energy loss per wavelength and expressed as 2π times the ratio of the energy stored to the energy lost in the material per cycle (e.g., Ref. [30]).

Leaving aside the contribution of the reduction of energy intensity in the wavefield with increasing distance (i.e., geometrical spreading) without loss of generality, [74] indicated the effective total Q (Q_{tot}) as the sum of anelastic attenuation and scattering [19]:

$$\frac{1}{Q_{tot}} = \frac{1}{Q_i} + \frac{1}{Q_{sc}} \tag{1}$$

where Q_{tot} represents the total (observed) quality factor, Q_i is the intrinsic (or anelastic) quality factor, and Q_{sc} is the scattering quality factor, a parameter introduced by Ref. [2] to make scattering-related and anelastic energy losses comparable to one another. The anelastic effect represents the transformation of elastic energy into heat or other forms of energy due to material absorption or friction. The scattering effect is related to the interaction of the wave field with the material heterogeneities.

In a soft sedimentary cover, the Q factor – which here can indicate either the compressional-wave quality factor (Q_P) or the shear-wave quality factor (Q_S) depending on the context – counteracts the effect of amplification due to impedance variations. Thus, Q, together with V_S, is a relevant parameter necessary to accurately estimate the site response through numerical simulations (e.g., Ref. [57]). The estimation of Q from empirical data, however, is not simple.

Some studies focusing on the estimation of Q_{tot} or Q_i in shallow geological layers took advantage of the availability of data recorded in vertical arrays of sensors where earthquake recordings were collected (e.g., Refs. [10,11,24,59,67]). [21] developed the peak-frequency method

* Corresponding author.
E-mail address: idreossi@ogs.it (I. Dreossi).

https://doi.org/10.1016/j.soildyn.2022.107387
Received 5 March 2022; Received in revised form 27 May 2022; Accepted 6 June 2022
Available online 8 July 2022

for calculating Q_i from direct waves of microseismic events. The method was improved and benchmarked by Refs. [75,76] and used by Ref. [20]. Other works have proposed estimating Q_{tot} or Q_i by considering active seismic source recordings [25,31,73,80,81]. Among those studies, attempts were made to exploit the amplitude versus offset analysis (e.g., Ref. [85]), but also some works involved combining amplitude decay, spectral ratios, Wiener filters, and artificial neural networks (Ref. [83]). In addition, [17] carried out seismic interferometry by cross-correlation in a borehole.

The passive technique based on ambient seismic noise analysis can also be used to assess the seismic response of a site and allows characterization with a high spatial coverage even of areas with moderate or low seismicity. While this technique has been widely and successfully adopted for retrieving V_S profiles (e.g. Refs. [1,8,9,14,23,43,56,61,68]), less attention was paid to its potential in providing an estimate of the Q factor below a site. Attempts to estimate the attenuation coefficients from ambient seismic noise have been carried out at both regional (e.g., Refs. [4,44–48,51,54,65,66,70,77]) and local scales (e.g., Ref. [3]). In particular, by focusing on Q_S at a local scale, [58] proposed a scheme for the attenuation factor inversion aimed at retrieving the 1D Q_S structure below a site from ambient seismic noise once the V_S profile from the inversion of dispersion curves was known independently. The inversion was based on a least-squares algorithm with an attenuation positivity constraint (e.g., Ref. [50]). The results provided from this method for the shallowest geological layers are valuable, as was demonstrated for test sites where independent Q_S estimates were available (e.g., Refs. [12,15,58]). However, the procedure requires a careful trial and error testing of the damping factors to obtain robust solutions.

In this paper, the approach proposed in Ref. [58] was modified by exploring the potential of the Simultaneous Algebraic Reconstruction Technique (SART) to avoid the preliminary analysis required by the least-squares algorithm. First, a description of the SART algorithm and the way it is used for the case at hand is provided. Second, two test sites analyzed in previous publications and here adopted for refining the results gained with SART are considered, and a summary of the analyses conducted is given. At both the considered test sites, the Q_S obtained in this study is compared with the Q_S calculated with the procedure proposed in Ref. [58], and their effect on the expected ground motion at the surface is estimated by calculating the deconvolved wave field from synthetic seismograms of vertically propagating S-waves. Suggestions regarding the choice of the inversion parameters (i.e., the number of iterations and the relaxation parameter) for estimating Q_S using SART are also presented. Finally, the inversion procedure is applied to data collected at the Piana di Toppo (PITOP) test site, northeastern Italy, where independent geophysical measurements were carried out.

2. Method

The estimation of the Q_S factor was carried out in two steps that follow the approach described in Ref. [58] and are briefly summarized here.

In the first step, the S-wave velocity profile was calculated by the inversion of the Rayleigh-wave phase velocity dispersion curve, and the attenuation coefficients were estimated using a modified version of the Extended Spatial AutoCorrelation (ESAC) approach [55,61]. Using this method, the frequency-dependent Rayleigh-wave phase velocity is estimated by the frequency domain fit of the theoretical Bessel functions to the empirical correlation coefficients [1]. In order to consider the effect of inelasticity, [66] introduced adjustments to the equation originally proposed for the propagation of the waves in an elastic medium. Therefore, in this study, the phase velocity and the frequency-dependent attenuation factor at a local scale are estimated via a grid search procedure [58] by using the modified equation presented in Ref. [66]. Moreover, an inversion only for the dispersion curve of phase velocity was carried out to obtain the *Vs* profile.

In the second step, Q_S was estimated from the inversion of the attenuation coefficients by constraining V_S to the values obtained in the first step. While the Rayleigh wave attenuation factor of the input data is frequency-dependent, the Q_S of the layered model is assumed frequency-independent. The attenuation coefficients of Rayleigh waves are related to Q_P and Q_S of a layered model by (Ref. [6]):

$$\alpha(\omega) = \frac{\omega}{2c(\omega)^2}\left[\sum_{i=1}^{M} v_{Pi}\frac{\delta c(\omega)}{\delta v_{Pi}}Q_{Pi}^{-1} + \sum_{i=1}^{M} v_{Si}\frac{\delta c(\omega)}{\delta v_{Si}}Q_{Si}^{-1}\right] \quad (2)$$

where $\alpha(\omega)$ is the Rayleigh wave attenuation factor dependent on frequency, ω is the angular frequency, $c(\omega)$ represents the phase velocity, and M is the total number of layers of the subsoil model. V_{Pi} and V_{Si} are the compressional- and the shear-wave velocities of the ith layer, respectively. $Q_{Pi}^{(-1)}$ and $Q_{Si}^{(-1)}$ indicate the inverse of the compressional-wave quality factor of the ith layer and the inverse of the shear-wave quality factor of the ith layer, respectively.

If V_S/V_P is less than 0.45, the analyses can be performed by inverting only Q_S [81] and the formula simplifies to:

$$\alpha(\omega) = \frac{\omega}{2c(\omega)^2}\left[\sum_{i=1}^{M} v_{Si}\frac{\delta c(\omega)}{\delta v_{Si}}Q_{Si}^{-1}\right] \quad (3)$$

When several frequencies are considered during the quality factor inversion process, a system of linear equations with the attenuation coefficients as data and the Q values as unknowns can be solved. In this paper, the estimation of Q_S was carried out with SART. In particular, Q_i was estimated assuming that the contribution of Q_{sc} was negligible, since the interstation distances of the microarray are smaller than the wavelengths of seismic waves.

2.1. Simultaneous Algebraic Reconstruction Technique (SART)

SART was proposed by Ref. [5] as a superior implementation of the Algebraic Reconstruction Technique (ART).

ART was first employed in the 1970s by Ref. [29] for X-ray photography in radiology and electron microscopy, with the aim of solving the problem of the direct 3D reconstruction of an object. Weighted sums of appropriate reconstruction elements are combined in ART with the respective projection data in an iterative way [28,29].

It soon emerged that ART presented salt and pepper noise problems in the reconstructions. For this reason, [27] proposed an alternative computer implementation called Simultaneous Iterative Reconstruction Techniques (SIRT). SIRT was designed to provide the correct reconstructions of 3D objects in electron microscopy [27]. Although improving the resulting image resolution with respect to ART, the time necessary for gaining the convergence and, consequently, for image reconstruction is generally longer than with ART [41].

When SART was introduced in the 1980s, it appeared to bring together the best features of both ART and SIRT techniques, which are the rapid convergence of the first and the higher resolution of the second. SART also succeeds in suppressing noise, which is the main quality of SIRT. This means that the reconstructions are smoother than those achieved using ART, since the contrasting and constant unknown update is removed at every new equation [41]. [5] highlighted a further advantage. Based on weighted sums of rows and columns of the input data kernel matrix, SART applies at the same time to a single unknown the average of the corrections generated by all rows in one projection. This differs from ART, which updates the unknown values sequentially row-by-row.

As SART is based on weighted averages, it implies that the results depend strictly on the weight that each value has inside the data kernel matrix. Moreover, correcting each unknown for all rows at once means a faster convergence than for ART. Furthermore, SART can also be used for solving linear problems by constraining the space of the solutions. The high resolution, together with the possibility of implementing constraints on the solution of a linear problem easily, seems to make

SART a suitable algorithm for estimating the quality factor following the approach of [58].

Let us consider a linear inverse problem expressed in matrix-vector notation:

$$Af = d \tag{4}$$

where A is the N X M data kernel matrix, f is a vector containing the M unknown model parameters, and d represents the data vector of N measurements [50]. This paper computes $1/Q$. Considering that the Q factor cannot be negative, but in some layers the calculated $1/Q$ values could be thus estimated, when analyzing experimental data it is necessary that an additional constraint $1/Q > 0$ is fixed as a condition on the smoothing [42]. Alternatively, more generally concerning $1/Q$, it could be necessary to fit the data within some confidence bound (see Refs. [71,72]) as:

$$d - \eta \leqslant Af \leqslant d + \eta \tag{5}$$

where η is a vector containing predetermined confidence intervals. In the present study, an additional constraint $1/Q > 0$ (in this case, in solving equation (3)), rather than confidence intervals was used.

When considering equation (3), equation (4) becomes the following:

$$\begin{bmatrix} \frac{\omega_1}{2c(\omega_1)^2} v_{S1} \frac{\delta c(\omega_1)}{\delta v_{S1}} \cdots & \frac{\omega_1}{2c(\omega_1)^2} v_{SM} \frac{\delta c(\omega_1)}{\delta v_{SM}} \\ \cdot & \cdot \\ \cdot & \cdot \\ \cdot & \cdot \\ \frac{\omega_N}{2c(\omega_N)^2} v_{S1} \frac{\delta c(\omega_N)}{\delta v_{S1}} \cdots & \frac{\omega_N}{2c(\omega_N)^2} v_{SM} \frac{\delta c(\omega_N)}{\delta v_{SM}} \end{bmatrix} \cdot \begin{bmatrix} Q_{S1}^{-1} \\ \cdot \\ \cdot \\ \cdot \\ Q_{SM}^{-1} \end{bmatrix} = \begin{bmatrix} \alpha(\omega_1) \\ \cdot \\ \cdot \\ \cdot \\ \alpha(\omega_N) \end{bmatrix} \tag{6}$$

where the data kernel matrix A considers the contribution of V_S to the attenuation factors, M is the number of layers of the selected model, and N stands for the number of attenuation factors adopted, which is equal to a sufficient number of frequencies selected from the original dataset that is able to define the trend in the curve of the attenuation factors.

The solution is calculated by SART as follows:

$$f_j^{(k+1)} = f_j^{(k)} + \lambda \frac{\sum_{i=1}^{N} \left[\frac{p_i - \sum_{j=1}^{M} A_{ij} f_j^{(k)}}{\sum_{j=1}^{M} A_{ij}} \right] A_{ij}}{\sum_{i=1}^{N} A_{ij}} \tag{7}$$

where $f_j^{(k+1)}$ is the new estimate of the inverse of the quality factor Q_{sj}^{-1}, $f_j^{(k)}$ is the current estimate of the inverse of the quality factor Q_{sj}^{-1}, and k stands for the kth SART iteration. The index i is the row number and represents the data considered, which are linked to the frequencies selected from the original dataset for defining the curve of the attenuation factors. The index j is the column number and stands for the unknowns, which are the number of layers of the subsoil model considered for the site analyzed. A is the matrix of partial derivatives of V_S. $\sum_{i=1}^{N} A_{ij} f_j^{(k)}$ returns the retrieved attenuation factor, p_i is the observed attenuation factor, and λ is the relaxation parameter, which helps in mitigating the noise.

[5] commented that one iteration of SART is sufficient to generate a good reconstruction in terms of quality and numerical accuracy. Furthermore, they pointed out that the under-relaxation (i.e., $\lambda < 1$) proposed for the ART technique by some authors [28,34–37,69] increased the number of iterations for a solution to converge and decreased noise in the solution.

In this work, it was investigated as to whether, with a certain combination of SART parameters, including λ, an acceptable balance between the number of iterations and the quality of the reconstructions is achieved by means of reliability tests.

3. Reliability tests

In the Q_S inversion process with SART the influence of varying λ, the number of SART iterations, and the attenuation positivity constraint on the solution was tested. To estimate the range of parameters that allow obtaining robust solutions, the inversion was carried out at test sites where the quality factor was known either from independent measurements or from previous ambient seismic noise inversions.

The first test site considered was at Telegrafenberg, located at the Alfred Einstein Science Park in Potsdam, Germany. The data set is the one used in Refs. [12,15] and is composed of ambient seismic noise recordings from a sparse array geometry. 18 stations equipped with a GFZ-WISE system – namely, low-cost digitizers generating wireless mesh networks [22,62] – and 4.5 Hz sensors recorded simultaneously for more than 1 h at 100 samples/sec. Minimum and maximum interstation distances were 4.0 m and 45.0 m, respectively. Only the vertical component of the recording of each station was analyzed and it was divided into 30-s non-overlapping windows. Each signal window was tapered for 5% of its length at both ends by means of a cosine function to minimize leakage problems. After that, the spatial correlation coefficients were calculated in the same way as in Ref. [58]. The frequency band considered is 2.51–9.45 Hz. More information on data acquisition and analyses can be found in Refs. [12,15].

The second test site is the village of Tito, in the Saint Loja Plain near the town of Potenza (Basilicata region), southern Italy. In this case, the data consist of ambient seismic noise recordings from a non-regular array configuration. 11 stations equipped with a 24-bit digitizer connected to a Mark L-4C 3D 1Hz sensor and a Global Positioning System (GPS) recorded simultaneously for more than 1 h at 500 samples/sec. Minimum and maximum interstation distances were 5.1 m and 66.8 m, respectively. Only the vertical component of the recording of each station was analyzed and it was divided into 60-s non-overlapping windows. Each signal window was tapered for 5% of its length at both ends by means of a cosine function to minimize leakage. The frequency range used is 3.25–10.64 Hz. More information on this second data set can be found in Ref. [60] – specifically, their array 1 – and in Ref. [58].

The V_S model of Telegrafenberg consists of four layers to a depth of 47 m [12]. The model for the Tito test site provides information on the velocity structure down to 35 m depth and is subdivided into five layers [58]. Both [12,58] calculated the 1D V_S profile following the inversion adopted in Ref. [61] using the modified genetic algorithm by Ref. [82]. Then, they retrieved the intrinsic Q_S following the original procedure proposed by Ref. [58]. Due to a V_S/V_P ratio less than 0.45, the inversion process in Ref. [12] and in Ref. [58] was calculated using Eq. (3). V_S and Q_S values retrieved by Ref. [12] and by Ref. [58], respectively, are shown in Table 1. At the Tito test site, [53] estimated a damping of less

Table 1
Q_S values versus depth for (a) the Telegrafenberg test site by Ref. [12] and (b) the Tito test site by Ref. [58].

(a) Telegrafenberg test site.

Layer	Thickness [m]	V_S [m/s][a]	Q_S[b]
1	7	175	15.0
2	9	235	14.9
3	21	301	16.4
4	10	310	76.2

(b) Tito test site.

Layer	Thickness [m]	V_S [m/s][a]	Q_S[b]
1	6.9	202	9.8
2	8.5	190	11.2
3	5.4	212	50.1
4	10.4	310	13.9
5		324	7.7

[a] Shear-wave velocity.
[b] Shear-wave quality factor.

than 5% [i.e., considering a Q_S larger than 10 in the relation damping = $1/(2Q_S)$] between about 1 and 2.5 Hz by using a non-parametric analysis of a M = 2.8 earthquake occurred in Southern Apennines (Italy). Further geophysical Q_S values at the Tito test site were obtained from down-hole measurements by Ref. [60], who analyzed S-waves at intervals of 1 m down to 30-m depth generated by a 7-kg sledgehammer hitting horizontally a steel plate at the surface. The acquisition system consisted of a 16-bit digitizer and one 10-Hz down-hole geophone recording at 4000 samples/sec. The analyses were performed by Ref. [60] adopting the spectral amplitude decay analysis and the spectral ratio technique [26]. With the former method, [60] estimated a Q_S factor equal to 7 at 30 Hz, around 7.5–15 between 35 and 45 Hz, and about 20–30 between 50 and 80 Hz. The latter method provided Q_S values in the range 10–20 – thereby, consistent with the Q_S retrieved using the spectral amplitude decay analysis – by fitting the frequency bands 15–40 Hz and 15–50 Hz of the down-hole data collected from between 5 and 25 m depth. In this work, tests at both sites were carried out using Eq. (3) to compare the parameter Q_S estimated with the original algorithm and the Q_S retrieved using SART. The Q_S profiles of [12,58] for the Telegrafenberg and Tito test sites, respectively, are regarded as the references, since they are published values gained using the approach of [58]. Furthermore, in the case of the Tito test site, the Q_S values in Ref. [58] were also compared with the results of other geophysical methods.

The starting models for the 1D Q_S inversion were that of [12] for the Telegrafenberg test site and of [58] for the Tito test site, respectively, and are shown in Table 1. The dispersion curves of [12,58] were used as input data, as well.

In the first step of the testing procedure, the model resolution matrix was calculated, in order to estimate the appropriateness of the model parametrization and to decide the number of layers to be considered in the analysis. Indeed, the model resolution matrix provides information on whether and how the model parameters can be solved [50]. The nearer the resolution matrix gets to the identity matrix, the higher the quality of the inversion [40]. The over-determined problem was resolved using the Singular Value Decomposition (SVD) [79] to estimate the model resolution matrix. The data kernel matrix (or Jacobian matrix), which is the matrix of partial derivatives of velocities, was also considered for a first validation of the parametrization and the quality of the data.

In order to estimate the influence of the choice of the inversion parameters on the solution and to define criteria for the final inversion of the data, the inversion was carried out several times varying the λ value within the range 0.1–2.0 with a step of 0.1, while a maximum number of 200 iterations was tested.

The Root Mean Square (RMS) of the difference between the observed and calculated attenuation coefficients (i.e., the residuals) was estimated at each iteration and for each value of λ. The same was done for the perturbation of the solution (P) at each SART iteration with respect to the starting solution, calculated according to the following formula [84]:

$$P = \frac{1}{M}\sum_{j=1}^{M}\left(f_{j(k^{th})} - f_{j(starting\ value)}\right)^2 \quad (8)$$

where M stands for the total number of layers of the subsoil model considered for the Q_S inversion, $f_j(^{th}_k)$ represents f_j at the kth SART iteration, and $f_{j(starting\ value)}$ is the starting f_j at the first SART iteration. The optimal number of iterations was defined as that leading to the best compromise between the RMS of the residuals and P.

Then, the effect of the attenuation positivity constraint on the solutions, and if this parameter was mandatory for a non-negative Q_S estimation, was investigated. Two diverse attenuation positivity constraints were assumed for the different tests. In one instance, the attenuation positivity constraint forced the solution at each iteration to re-set $1/Q_S$ equal to 0 (i.e., a condition of perfect elasticity) in case it gave a negative result. Alternatively, the solution was forced to be equal to 1/5, again in case it resulted negative or greater than 1/5, restricting the space of the solution. This is because no values lower than 5 were expected either at the Telegrafenberg [12] or Tito [58] test sites.

For each combination of parameters, the estimated attenuation factors were then compared with the observed attenuation factors already obtained at these sites. The starting f_j value was set to 0.

3.1. Telegrafenberg test site

Fig. 1a shows that the model resolution matrix calculated with the same 1D V_S set up model of [12] can be predicted well in the first three layers, similarly to what observed from the Jacobian matrix (see Ref. [12]). In fact, it is diagonal for the first three layers, thus indicating a reliable prediction of the Q_S value. For the fourth layer, on the contrary, the resolution is poor, so that this last layer cannot be well predicted. This information will be considered when comparing the results of the inversions.

Fig. 2 depicts the retrieved attenuation factors at each of the 200 SART iterations and compares them with the observed attenuation factors of [12], first for $\lambda < 1$, and then for $\lambda > 1$. On the left (Fig. 2a, $\lambda < 1$) the retrieved attenuation factor converges gradually towards the observed one. This is consistent with the expectation that lower values of λ lead to a slow convergence versus the minimum of the solution. Fig. 2b (right panel, $\lambda > 1$) shows a non-regular trend in the convergence. A λ equal to 1.8 guarantees almost an immediate adjustment of the solution, but this results in its overall instability. In general, inversions carried out with λ larger than 1.0 resulted in increasingly unstable solutions.

In Fig. 3, the RMS (graph on the left) and the perturbation (P) (graph in the middle) of a solution with an initial f_j value equal to 0 and no attenuation positivity constraint are represented for λ values in the range 0.1–2.0. A focus on a maximum of 50 SART iterations is provided, since beyond this number no appreciable variations were encountered. For λ increasing from 0.1 to 1, the number of SART iterations required for the RMS to stabilize are progressively lower; vice versa for λ increasing from 1.0 to 2.0, with 2.0 being an unacceptable value. However, a slow convergence is often preferable [33]. On the other hand, the lowest P values are gained for less than 20 SART iterations and $\lambda < 1$. The area that falls within the yellow dashed line represents a good compromise between the best RMS and P values. Within this area, no negative Q_S values were obtained. In addition, within the same highlighted area, the attenuation positivity constraint for which the solution was forced to be equal to 1/5 was not needed during the inversion process. In general, within the area of good compromise, the solutions for different combinations of λ and SART iterations tend to have similar values to each other. Although a good compromise between the RMS and P can be observed when $\lambda > 1$, values of $\lambda < 1$ were preferred because they provide a gradual convergence of the solution, consistent with λ values in the literature (e.g., Refs. [5,16,28,39]). For both the graph on the left and in the middle, a combination of parameters was chosen – that is λ equal to 0.4 and 30 SART iterations –, in view of applying it to the inversion at the PITOP test site without conducting prior reliability tests. The value 0.4 of λ provides a rather slow but gradual convergence of the solution, whereas 30 SART iterations ensure that the solution stabilizes. The corresponding 1D Q_S profile with depth is shown in the graph on the right. The 1D Q_S profile by Ref. [12] is shown for comparison. Q_S in the first three layers is similar to that calculated by Ref. [12], whereas the last layer (not constrained, as indicated by the model resolution matrix, Fig. 1a) shows a lower value. Occasionally, when λ was equal to 2.0 (generally, this is not a suggested value in literature) negative or infinite Q_S values were found.

Finally, the impulse response of the model of [12] and the model obtained in this study were compared. Fig. 4a and b shows the deconvolved wave field calculated from synthetic S-wave seismograms at the soil surface and at a depth equal to the soil thickness of the 1D Q_S model of Telegrafenberg test site, respectively. The soil surface is used as the reference in the deconvolution procedure. Specifically, Fig. 4a is

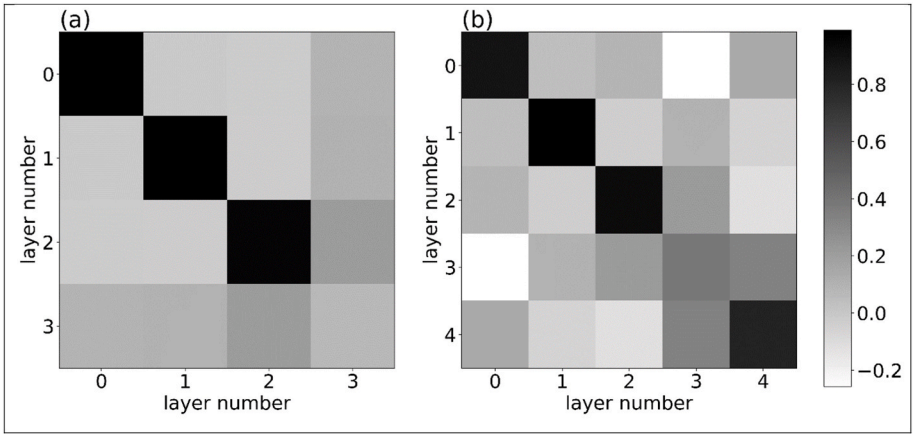

Fig. 1. Resolution matrix calculated for the (a) Telegrafenberg and (b) Tito test sites by adopting the same starting setup model of [12,58], respectively. The numbering of the x and y axes at the bottom and on the left of each matrix correspond to the layers of each model, where in (a) 0 indicates the shallowest layer and 3 the deepest one, and in (b) 0 indicates the shallowest layer and 4 the deepest one. The color palette covers the range of values assumed by the cells. In (a) the minimum and maximum values are −0.024 and 0.990, respectively. In (b) the minimum and maximum values are −0.257 and 0.982, respectively.

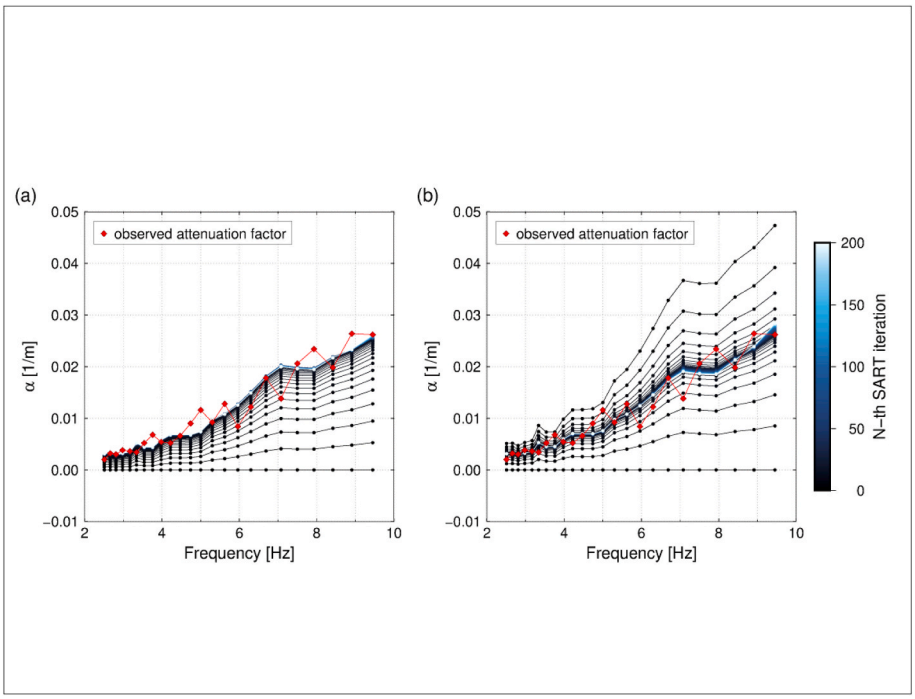

Fig. 2. Observed and retrieved attenuation factors versus frequency for the Telegrafenberg test site, obtained by fixing a starting f_j equal to 0, with no attenuation positivity constraint, and 200 SART iterations. Red diamonds represent the observed attenuation factors. The color palette distinguishes the number of SART iterations. The relaxation parameters chosen are (a) $\lambda = 0.2$ and (b) $\lambda = 1.8$. It can be seen that in (a) the retrieved attenuation factors converge progressively towards the observed ones, whereas in (b) the convergence is not stable.

obtained considering the Q_S values retrieved with SART (black line) as input, whereas Fig. 4b is retrieved from the original Q_S values (red line) by Ref. [12]. The difference between Fig. 4a and b is small and probably related to the diverse values of the last layer, which is poorly solved.

3.2. Tito test site

Fig. 1b shows the model resolution matrix calculated with the same 1D V_S set up model adopted by Ref. [58]. The shallowest three layers of the model are predicted rather well, whereas the fourth suffers from limited resolution and trade-off. Then, in the fifth layer, the resolution increases again.

In Fig. 5, the RMS (graph on the left) and P (graph in the middle) of a solution with an initial f_j value equal to 0 and no attenuation positivity constraint, are shown for λ in the range 0.1–2.0. Consistent with the Telegrafenberg test site, a focus on a maximum of 50 SART iterations is given. Differently from the previous test site, some anomalies were encountered for a high number of SART iterations, as discussed later in this section. When λ has a low value the solution converges slowly, so more iterations are required for the RMS to stabilize, as would be expected. The opposite occurs when λ increases from 1.0 to 2.0, with 2.0 being an unacceptable value. With respect to P, the lowest values are achieved for less than 10 SART iterations and $\lambda < 1$. The area that falls within the yellow dashed line indicates what the preferable compromise between the best RMS and P values is. Also at this test site, within this area no negative Q_S values were obtained. Again, within the same highlighted area, the attenuation positivity constraint for which the solution was forced to be equal to 1/5 was not needed during the inversion procedure. Moreover, within the area of good compromise, the solutions for diverse combinations of λ and SART iterations tend to be close to one another. Even if acceptable values can be observed when $\lambda > 1$, values of $\lambda < 1$ were preferred, in accordance with the literature, since in such a way the solution can converge gradually. For both the graph on the left and in the middle, the same combination of parameters of the Telegrafenberg test site was selected – that is λ equal to 0.4 and 30 SART iterations –, always in the perspective of using it for the inversion at the PITOP test site. The corresponding 1D Q_S profile with depth is shown in the graph on the right, where the 1D Q_S profile by Ref. [58] is depicted for comparison. Q_S is very similar to that calculated by Ref. [58]. Occasionally, outside the area highlighted in yellow in Fig. 5,

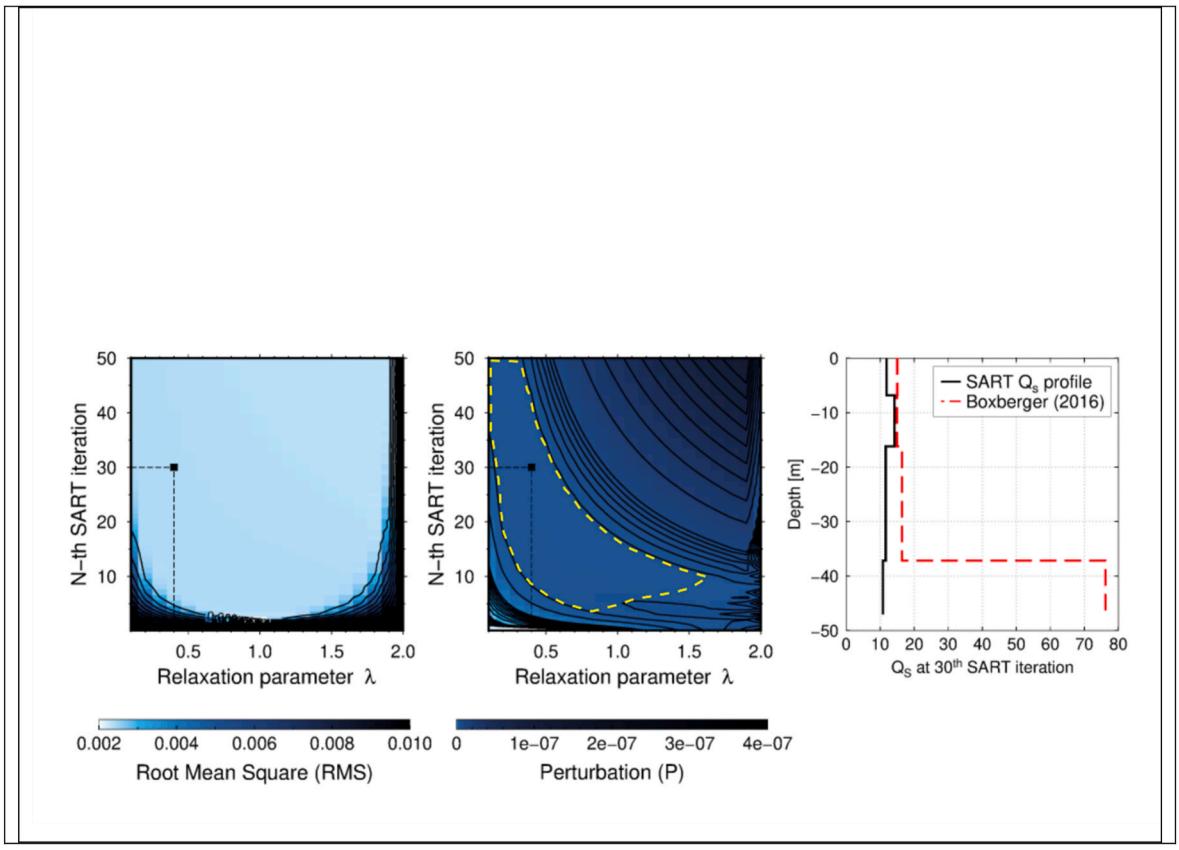

Fig. 3. Telegrafenberg test site. On the left, variation of the Root Mean Square (RMS) for all tested λ, no attenuation positivity constraint and a maximum number of 50 SART iterations, when the starting f_j is equal to 0. In the middle, variation of the perturbation (P) for all tested λ, no attenuation positivity constraint, and a maximum number of 50 SART iterations, when the starting f_j is equal to 0. The yellow dashed line indicates the area of best compromise between this graph and the one on the left. On the right, 1D Q_S profile obtained when λ is set equal to 0.4 at the 30th SART iteration. The values of RMS and P calculated with the same combination of parameters are indicated with a black square in the graph on the right and in the middle, respectively. The profile of [12] is shown with a red dashed line.

when more than 90 SART iterations were run and $\lambda \geq 0.9$ (generally, these values are not suggested in literature), a negative Q_S was encountered.

In Fig. 4c and d the deconvolved wave field estimated from synthetic S-wave seismograms at the soil surface and at a depth equal to the soil thickness of the 1D Q_S model of the Tito test site, respectively, are shown. Fig. 4c, in particular, is retrieved from the 1D Q_S model estimated in this work. Fig. 4d, instead, considers the original 1D Q_S model by Ref. [58]. The soil surface is taken as the reference in the deconvolution process. Also for this test site, the results generated by the two different inputs are comparable, showing that the effect of the small differences in the estimated models is negligible.

4. Application to the Piana di Toppo (PITOP) test site

PITOP is the borehole geophysical testing site of the National Institute of Oceanography and Applied Geophysics – OGS (OGS). It is a free field rectangular area of around 4500 m^2 located at Piana di Toppo in the Toppo inter-mountain plain (municipality of Travesio, Friuli Venezia Giulia region), northeastern Italy. The test site lies on Quaternary loose coarse gravels overlying conglomerates (*Montello conglomerate,* Miocene formation) [64]. Here three boreholes were drilled down to a depth of 280 m ("well 1"), 380 m ("well 2"), and 422 m ("well 3"). V_P and V_S profiles were retrieved from sonic logs integrated with Vertical Seismic Profiling (VSP) [64]. An average P-wave quality factor (Q_P) value, equal to 28, of the 1D Q_P profile obtained considering "well 2" and "well 3" was also estimated using two methods [63]. The first was the spectral ratio method, which measures the variation of the amplitude spectrum in the VSP down-going P-wave signal (direct) at different depths. The second adopts the signal dispersion analysis for estimating the attenuation. The estimate is achieved by comparing the velocities retrieved from sonic logs that use a signal frequency of several thousand Hz, and VSP, characterized by a signal frequency of around 50 Hz. Both methods consider the variation of the signal over a depth range between 100 m and 380 m (F. Poletto, personal communication, November 8th, 2020). The relationship between Q_P and Q_S in sediments varies appreciably in the literature (e.g., Refs. [18,49,52]), so the average Q_S value was retrieved in general terms from the following relation [6], by assuming that the subsoil investigated is an isotropic Poisson solid:

$$\frac{Q_P}{Q_S} = \frac{9}{4} \tag{9}$$

giving an average Q_S value equal to 12.44.

In this study, an ambient seismic noise measurement campaign in array configuration was realized at the PITOP test site. 11 Sentinel-GEO Seismic stations (Lunitek) that integrate a triaxial 85 dB MEMS accelerometer plus a triaxial set of 4.5 Hz geophones, as well as GNSS receiver and WiFi module, were deployed in three concentric circles. The minimum, median, and maximum approximate radii of the array were 5.1 m, 14.9 m, and 33.6 m, respectively. Minimum and maximum interstation distances were 5.0 m and 80.9 m, respectively. The stations recorded simultaneously for more than 2 h at 250 samples/sec. The acquisition of the point position was performed with a GNSS SoluTOP MS1 system (SoluTOP s.a.s.) using the software android open-source Qfield. Data points were sent in real time to a PostgreSQL database (PostGIS geospatial extension). After dividing the recording of the vertical

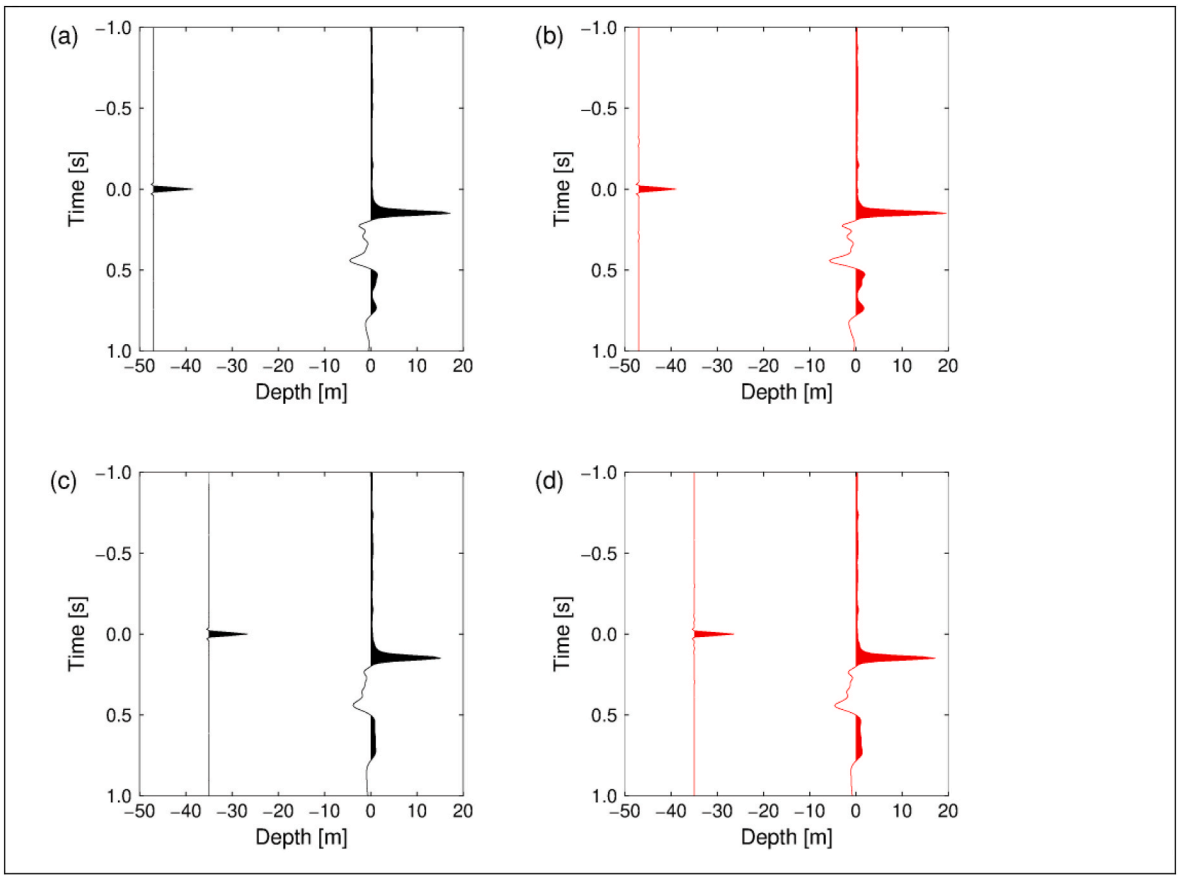

Fig. 4. Deconvolved wave field obtained from the synthetic S-wave seismograms at the soil surface and at a depth equal to the soil thickness of the 1D Q_S model calculated at the Telegrafenberg test site using (a) the Q_S values retrieved with SART (black line) and (b) the original Q_S values by Ref. [12] (red line), respectively, and at the Tito test site using (c) the Q_S values retrieved with SART (black line) and (d) the original Q_S values by Ref. [58] (red line), respectively. The soil surface is used as the reference.

component of each station into 60-s non-overlapping windows, and tapering each window for 5% of its length at both ends with a cosine function to reduce leakages, the spatial correlation coefficients were calculated in the same way as in Ref. [58].

4.1. Results

The inversion for obtaining the 1D V_S profile was performed following [61] utilizing the modified genetic algorithm proposed by Ref. [82]. Values of the Rayleigh-wave dispersion curve over the range 3.36–24.38 Hz were considered. Horizontal-to-vertical spectral ratios were not taken into account for the inversion, since the site response in the considered frequency range is almost flat. The inversion was performed considering the apparent dispersion curve because the dominance of the fundamental and higher modes varies with frequency, based on the considered V_S profile. For this reason, the observed dispersion curve of phase velocity has to be treated as apparent. The search of the genetic algorithm was done considering a population of 50 starting models and running 150 generations. The crossover rate, which is an operator that combines information of two (or more) "parent" selected models randomly, was fixed to 0.7. The mutation rate, i.e., the operator used to ensure a certain degree of diversity in the population, was set to 0.01. The inversion was repeated seven times by changing the initial random number (also called seed number). Indeed, this inversion has something of a probabilistic nature in that it adopts random numbers for gaining models next to a global optimum solution [61]. The average RMS of the differences between observed and calculated models for each generated model represents the misfit function, where the model giving the minimum misfit was denoted to be the optimal version. Fig. 6 shows the results of the V_S inversion, with the 1D V_S profile retrieved by Ref. [64] also depicted for comparison. The best model obtained by the inversion of the dispersion curve showed some differences with respect to that of [64]. Note that, while the former provides an average velocity structure below the array, the latter represents the velocity versus depth profile only nearby the borehole. This can affect the comparison, since the local stratigraphy is not homogeneous.

The estimation of Q was performed while considering the best V_S model. From the analysis of both the model resolution matrix and the Jacobian matrix (not shown here), the inversion was carried out only for the first three layers of the best V_S model. In this work, the analysis was focused on the estimation of Q_S. This is because for the first three layers of the best V_S model the V_S/V_P ratio was smaller than 0.45. The value of λ was fixed to 0.4 and 30 SART iterations were run. The initial f_j was set equal to 0. The attenuation positivity constraint was not imposed on the solutions. The Q_S results are presented in Table 2 and a good fit of the calculated attenuation factors to the ones observed was obtained. The 1D Q_S profile calculated using SART provided values of Q_S that are lower than the mean Q_S estimated by converting the average Q_P value of [63]. It should be pointed out that the latter was derived from the analysis of measurements taken over the depth range between 100 m and 380 m, therefore much deeper than the depth range investigated by the noise array. Considering this, it seems reasonable that the shallower layers might have lower values of Q_S, within a range close to what was observed at greater depths.

5. Discussion and conclusions

The solution achieved using the inversion technique proposed by

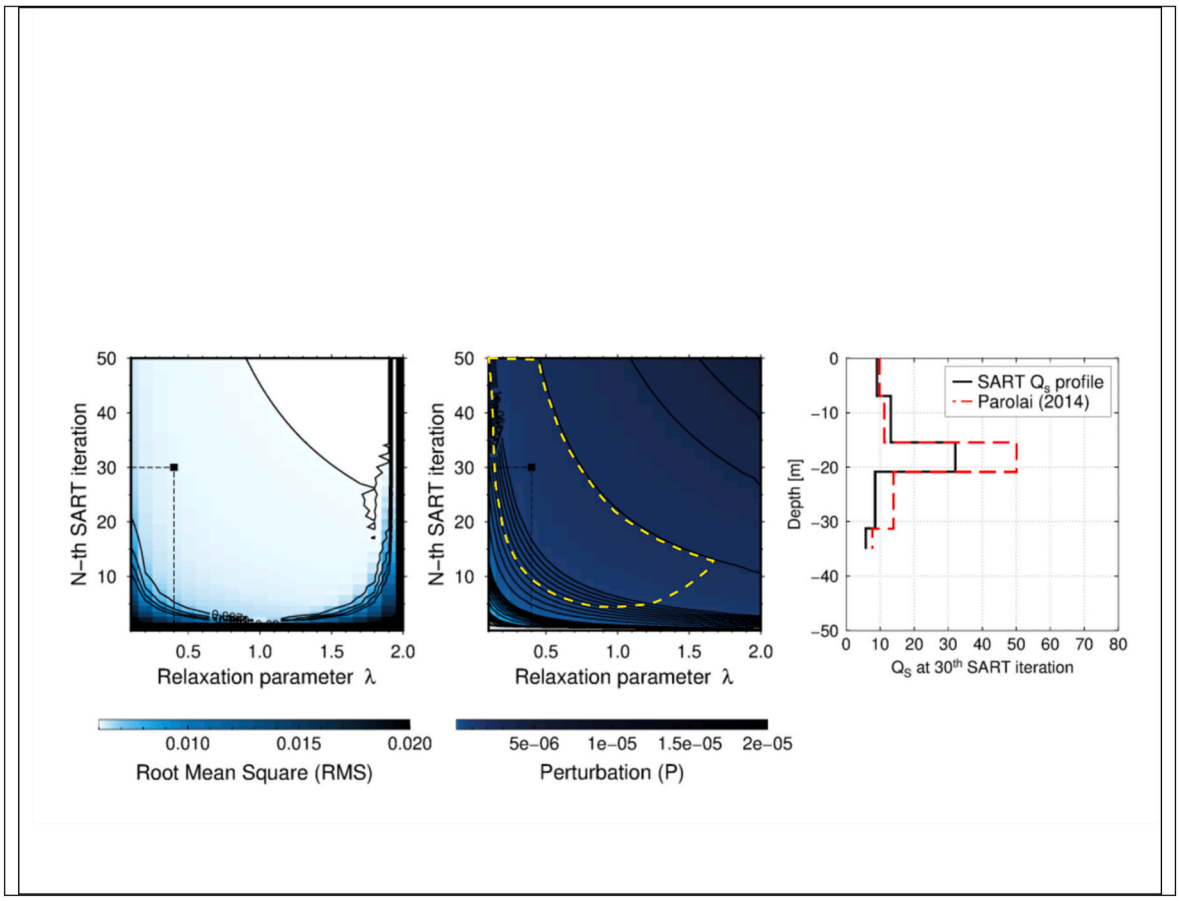

Fig. 5. Tito test site. On the left, variation of the Root Mean Square (RMS) for all tested λ, no attenuation positivity constraint and a maximum number of 50 SART iterations, when the starting f_j is equal to 0. In the middle, variation of the perturbation (P) for all tested λ, no attenuation positivity constraint, and a maximum number of 50 SART iterations, when the starting f_j is equal to 0. The yellow dashed line indicates the area of best compromise between this graph and the one on the left. On the right, 1D Q_S profile obtained when λ is set equal to 0.4 at the 30th SART iteration. The values of RMS and P calculated with the same combination of parameters is indicated with a black square in the graph on the right and in the middle, respectively. The profile of [58] is shown with a red dashed line.

Ref. [58], and based on a least-squares algorithm with attenuation positivity constraint (e.g., Ref. [50]), requires an accurate selection of the damping factors via a time-consuming trial and error procedure. In this work, the inversion of Q_S was carried out by replacing the least-squares algorithm with SART. SART is a suitable algorithm for linear inversions, and it offers the advantage of setting a positivity attenuation constraint to the solutions with ease.

The relaxation parameter λ, the number of SART iterations, and the attenuation positivity constraint, were the parameters tested for the 1D Q_S inversion at both the Telegrafenberg and Tito test sites. It was confirmed that $\lambda < 1.0$ let the solution converge gradually, proving robust Q_S values. Realistic results were also achieved with $\lambda > 1$, but the solution was unstable during the iterative process. For this reason, in the present work λ values lower than 1 were preferred, also in agreement with previous studies (e.g., Ref. [28]). Note that the computation time remains very limited, since the matrices considered in this work are small. The number of SART iterations required for the solution to converge – approximately, a minimum that goes from 5 to 30, depending on the selected λ – is acceptable since the inversion is very quick (i.e., of the order of a few seconds). This might also allow in the future to include a larger amount of data and, if justified by the resolution of the dispersion curves, of layers. The choice of both λ and the (small) number of SART iterations in the proposed approach, thus, can be done in a relatively wide range of values without substantially increasing the very rapid computation time or diminishing the convergence. The reliability tests at the two test sites highlighted that the attenuation positivity constraint was not necessary to avoid non-physical (negative Q) solutions for a wide combination of λ and number of SART iterations. This differs from the original inversion approach proposed by Ref. [58], for which the attenuation positivity constraint was mandatory. The analyses at both test sites showed that the Qs values obtained with SART are compatible with the original 1D Q_S models estimated using the inversion method by Ref. [58], but also with the data derived by independent geophysical measurements at the Tito test site. It is worth noting that this study was focused on deriving Q_S and does not treat the azimuthal distribution of ambient seismic noise sources. This latter aspect should be verified when analyzing data to accurately estimate both the phase velocity and seismic attenuation.

Finally, the application of the proposed approach to the PITOP test site showed encouraging results, which should be further validated by independent geophysical measurements carried out over the depth range investigated by the ambient seismic noise array.

5.1. Data and resources

Data from the Telegrafenberg test site were acquired by the Helmholtz Centre Potsdam GFZ German Research Centre for Geosciences using the Multi-Parameter wireless sensing system (MPwise) [13] seismic provided by the Geophysical Instrument Pool Potsdam (GIPP). Data from the Tito test site were collected as part of a scientific collaboration between the Helmholtz Centre Potsdam GFZ German Research Centre for Geosciences, the Università degli Studi della Basilicata, and the CNR-IMAA, which manages the Tito test site.

Seismic noise data acquired at the PITOP OGS geophysical test site

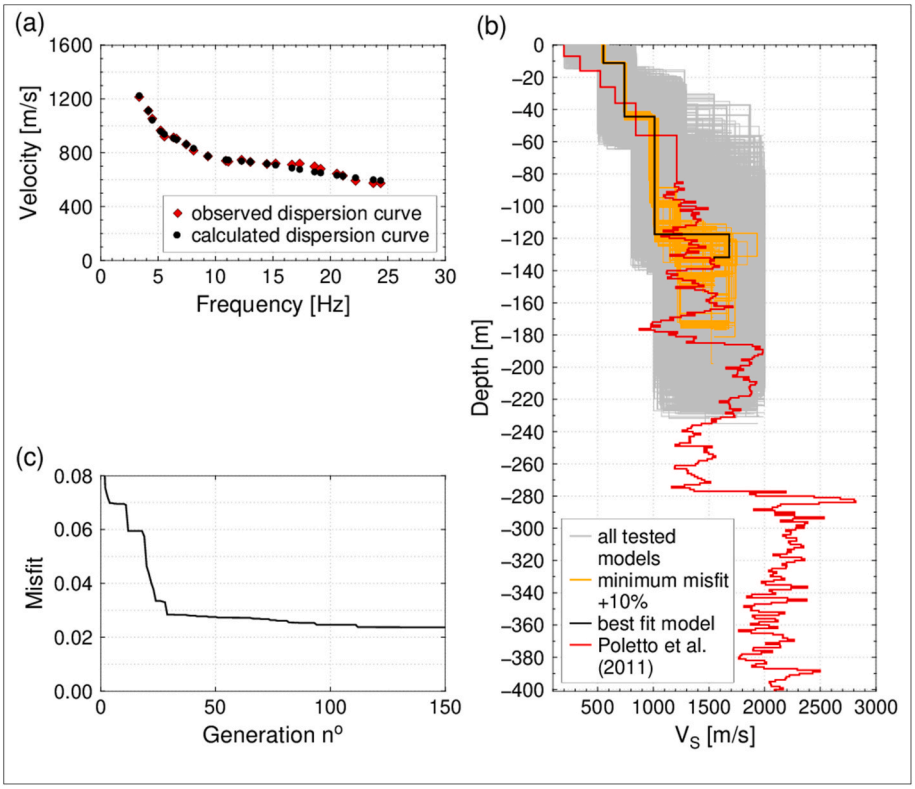

Fig. 6. V_S inversion results retrieved from the PITOP OGS geophysical test site. The inversion was performed considering the apparent Rayleigh wave dispersion curve. (a) Observed dispersion curve (red diamonds) and calculated Rayleigh wave dispersion curve (black circles). (b) 1D V_S profiles. The best-fitting model (black line), models in a range of 10% from the best model (orange lines), and all models tested (gray lines) are shown. The profile of [64] is indicated with a red line. (c) Misfit at each generation.

Table 2
1D Q_S profile for the PITOP OGS geophysical test site.

Layer	Thickness [m]	V_S [m/s][a]	Q_S[b]
1	11.1	551.4	5.7
2	33.2	741.6	4.4
3		1011.8	5.5

[a] Shear-wave velocity.
[b] Shear-wave quality factor.

are available at http://www.crs.ogs.it/archive/data_PITOP_noise/data_array_PITOP.tgz (last accessed 2022).

Fig. 1 was created with Python's libraries Matplotlib [38] and Numpy [32]. The remaining figures were produced using the Generic Mapping Tools (GMT), version 5.4.4 [78].

Author statement

Ilaria Dreossi: Conceptualization, Methodology, Software, Formal analysis, Investigation, Writing - Original Draft.

Stefano Parolai: Conceptualization, Methodology, Writing - Review and Editing.

Declaration of competing interest

The authors declare that they have no known competing financial interests or personal relationships that could have appeared to influence the work reported in this paper.

Acknowledgments

The authors thank the Helmholtz Centre Potsdam GFZ German Research Centre for Geosciences for providing both the Telegrafenberg and Tito test site data sets. Thanks to Flavio Poletto, Cinzia Bellezza and their OGS working group for providing the 1D V_S profile and the average Q_P value for the PITOP test site. Marco Severin (SoluTOP s.a.s.) kindly lent one GNSS SoluTOP MS1 system (SoluTOP s.a.s.) and gave assistance with the use of the instrument, the software android open-source Qfield, and the PostgreSQL database (PostGIS geospatial extension). The authors acknowledge Frank Rackwitz (Technische Universität Berlin) for his help and valuable suggestions. Thanks to the OGS colleagues for their support, in particular Carla Barnaba, Paolo Di Bartolomeo, and David Zuliani. Valerio Poggi helped in performing the ambient seismic noise measurements at the PITOP test site. Stephen Conway helped in improving the English, as well as Kevin Fleming, who also kindly provided useful comments on the manuscript. The authors also thank the Editor-in-Chief Hesham El Naggar, Fabian Bonilla, and the other two anonymous Reviewers for their constructive comments and suggestions. This study was supported by the agreement between the Regione del Veneto and OGS (Italy) (2020–2022).

References

[1] Aki K. Space and time spectra of stationary stochastic waves, with special reference to microtremors. Bull Earthq Res Inst 1957;35:415–56.
[2] Aki K. Scattering and attenuation of shear waves in the lithosphere. J Geophys Res 1980;85:6496–504. https://doi.org/10.1029/JB085iB11p06496.
[3] Albarello D, Baliva F. In-situ estimates of material damping from environmental noise measurements. In: Mucciarelli M, Herak M, Cassidy J, editors. Increasing seismic safety by combining engineering technologies and seismological data. Dordrecht: Springer; 2009. p. 73–84. https://doi.org/10.1007/978-1-4020-9196-4_6.
[4] Allmark C, Curtis A, Galetti E, de Ridder S. Seismic attenuation from ambient noise across the North Sea Ekofisk permanent array. J Geophys Res Solid Earth 2018; 123:8691–710. https://doi.org/10.1029/2017JB015419.
[5] Andersen AH, Kak AC. Simultaneous algebraic reconstruction technique (SART): a superior implementation of the ART algorithm. Ultrason Imag 1984;6:81–94. https://doi.org/10.1016/0161-7346(84)90008-7.
[6] Anderson D, Ben-Menahem A, Archambeau C. Attenuation of seismic energy in the upper mantle. J Geophys Res 1965;70:1441–8. https://doi.org/10.1029/JZ070i006p01441.
[7] Anderson JG. Physical processes that control strong ground motionSchubert G, editor. Treatise on geophysics, earthquake seismology 2007;5:513–65. Elsevier, Amsterdam.

[8] Arai H, Tokimatsu K. S-wave velocity profiling by inversion of microtremor H/V spectrum. Bull Seismol Soc Am 2004;94(1):53–63. https://doi.org/10.1785/0120030028.

[9] Arai H, Tokimatsu K. S-wave velocity profiling by joint inversion of microtremor dispersion curve and horizontal-to-vertical (H/V) spectrum. Bull Seismol Soc Am 2005;95:1766–78. https://doi.org/10.1785/0120040243.

[10] Assimaki D, Li W, Steidl JH, Tsuda K. Site amplification and attenuation via downhole array seismogram inversion: a comparative study of the 2003 Miyagi-Oki aftershock sequence. Bull Seismol Soc Am 2008;98(1):301–30. https://doi.org/10.1785/0120070030.

[11] Assimaki D, Steidl J, Liu PC. Attenuation and velocity structure for site response analyses via downhole seismogram inversion. Pure Appl Geophys 2006;163:81–118. https://doi.org/10.1007/s00024-005-0009-7.

[12] Boxberger T. A comparison of different seismological and geotechnical parameters for site characterization. Berlin, Germany: Genehmigte Dissertation, Technische Universität Berlin; 2016.

[13] Boxberger T, Fleming K, Pittore M, Parolai S, Pilz M, Mikulla S. The Multi-Parameter wireless sensing system (Mpwise): its description and application to earthquake risk mitigation. Sensors 2017;17:10. https://doi.org/10.3390/s17102400.

[14] Boxberger T, Picozzi M, Parolai S. Shallow geology characterization using Rayleigh and Love wave dispersion curves derived by seismic noise array measurements. J Appl Geophys 2011;75(2):345–54. https://doi.org/10.1016/j.jappgeo.2011.06.032.

[15] Boxberger T, Pilz M, Parolai S. Shear wave velocity versus quality factor: results from seismic noise recordings. Geophys J Int 2017;210:660–70. https://doi.org/10.1093/gji/ggx161.

[16] Censor Y, Eggermont PPB, Gordon D. Strong underrelaxation in Kaczmarz's method for inconsistent systems. Numer Math 1983;41:83–92. https://doi.org/10.1007/BF01396307.

[17] Cheng F, Draganov D, Xia J, Hu Y, Liu J. Q-estimation using seismic interferometry from vertical well data. J Appl Geophys 2018;159:16–22. https://doi.org/10.1016/j.jappgeo.2018.07.019.

[18] Clouser RH, Langston CA. Q_P-Q_S relations in a sedimentary basin using converted phases. Bull Seismol Soc Am 1991;81(3):733–50.

[19] Dainty AM. A scattering model to explain seismic Q observations in the lithosphere between 1 and 30 Hz. Geophys Res Lett 1981;8:1126–8.

[20] Drwiła M, Wcisło M, Anikiev D, Eisner L, Keller R. Passive seismic measurements of seismic attenuation in Delaware Basin. Lead Edge 2019;38:138–43. https://doi.org/10.1190/tle38020138.1.

[21] Eisner L, Gei D, Hallo M, Opršal I, Ali MY. The peak frequency of direct waves for microseismic events. Geophysics 2013;78:A45–9. https://doi.org/10.1190/geo2013-0197.1.

[22] Fleming K, Picozzi M, Milkereit C, Kühnlenz F, Lichtblau B, Fischer J, Zulfikar C, Özel O. SAFER, and E working groups. The self-organizing seismic early warning Information network (SOSEWIN). Seismol Res Lett 2009;80(5):755–71. https://doi.org/10.1785/gssrl.80.5.755.

[23] Foti S, Parolai S, Albarello D, Picozzi M. Application of surface-wave methods for seismic site characterization. Surv Geophys 2011;32:777–825. https://doi.org/10.1007/s10712-011-9134-2.

[24] Fukushima R, Nakahara H, Nishimura T. Estimating S-wave attenuation in sediments by deconvolution analysis of KiK-net borehole seismograms. Bull Seismol Soc Am 2016;106:552–9. https://doi.org/10.1785/0120150059.

[25] Gao L, Pan Y, Tian G, Xia J. Estimating Q factor from multi-mode shallow-seismic surface waves. Pure Appl Geophys 2018;175:2609–22. https://doi.org/10.1007/s00024-018-1828-7.

[26] Gibbs JF, Boore DM, Joyner WB, Fumal TE. The attenuation of seismic shear waves in Quaternary alluvium in Santa Clara Valley, California. Bull Seismol Soc Am 1994;84(1):76–90.

[27] Gilbert P. Iterative methods for the three-dimensional reconstruction of an object from projections. J Theor Biol 1972;36:105–17. https://doi.org/10.1016/0022-5193(72)90180-4.

[28] Gordon R. A tutorial on ART (algebraic reconstruction techniques). IEEE Trans Nucl Sci 1974;NS-21:78–93. https://doi.org/10.1109/TNS.1974.6499238.

[29] Gordon R, Bender R, Herman GT. Algebraic Reconstruction Technique (ART) for three-dimensional electron microscopy and x-ray photography. J Theor Biol 1970;29:471–81. https://doi.org/10.1016/0022-5193(70)90109-8.

[30] Green EI. The story of Q. Am Sci 1955;43:584–94.

[31] Haase AB, Stewart RR. Q-factor estimation. CREWES Research Report 2005;17.

[32] Harris CR, Millman KJ, van der Walt SJ, et al. Array programming with NumPy. Nature 2020;585:357–62. https://doi.org/10.1038/s41586-020-2649-2.

[33] Herman GT. A relaxation method for reconstructing objects from noisy X-rays. Math Program 1975;8:1–19. https://doi.org/10.1007/BF01580425.

[34] Herman GT. Image reconstruction from projections. In: The fundamentals of computerized tomography. New York-London: Academic Press; 1980.

[35] Herman GT, Lent A. Iterative reconstruction algorithms. Comput Biol Med 1976;6(4):273–94. https://doi.org/10.1016/0010-4825(76)90066-4.

[36] Herman GT, Lent A, Lutz PH. Relaxation methods for image reconstruction. Comm A C M 1978;21:152–8. https://doi.org/10.1145/359340.359351.

[37] Hounsfield GN. A method and apparatus for examination of a body by radiation such as X or Gamma radiation. Patent Specification 1283915; 1972. London (England).

[38] Hunter JD. Matplotlib: a 2D graphics environment. Comput Sci Eng 2007;9(3):90–5. https://doi.org/10.1109/MCSE.2007.55.

[39] Ivansson S. Seismic borehole tomography, theory and computational methods. Proc IEEE 1986;74:328–38. https://doi.org/10.1109/PROC.1986.13459.

[40] Jackson DD. Interpretation of inaccurate, insufficient and inconsistent data. Geophys J Int 1972;28(2):97–109. https://doi.org/10.1111/j.1365-246X.1972.tb06115.x.

[41] Kak AC, Slaney M. Principles of computerized tomographic imaging. IEEE Press; 1988.

[42] Knopoff L. Q. Rev Geophys 1964;2:625–60.

[43] Köhler A, Ohrnberger M, Scherbaum F, Wathelet M, Cornou C. Assessing the reliability of the modified three-component spatial autocorrelation technique. Geophys J Int 2007;168:779–96. https://doi.org/10.1111/j.1365-246X.2006.03253.x.

[44] Lawrence JF, Denolle M, Seats KJ, Prieto GA. A numeric evaluation of attenuation from ambient noise correlation functions. J Geophys Res 2013;118:6134–45. https://doi.org/10.1002/2012JB009513.

[45] Lawrence JF, Prieto GA. Attenuation tomography of the western United States from ambient seismic noise. J Geophys Res 2011;116:B06302. https://doi.org/10.1029/2010JB007836.

[46] Lin F-C, Ritzwoller MH, Shen W. On the reliability of attenuation measurements from ambient noise cross-correlations. Geophys Res Lett 2011;38:L11303. https://doi.org/10.1029/2011GL047366.

[47] Liu X, Ben-Zion Y, Zigone D. Extracting seismic attenuation coefficients from cross correlations of ambient noise at linear triplets of stations. Geophys J Int 2015;203(2):1149–63. https://doi.org/10.1093/gji/ggv357.

[48] Magrini F, Boschi L. Surface-wave attenuation from seismic ambient noise: numerical validation and application. J Geophys Res Solid Earth 2021;126:e2020JB019865. https://doi.org/10.1029/2020JB019865.

[49] Mandal P. Sediment thicknesses and Q_S vs. Q_P relations in the Kachchh Rift Basin, Gujarat, India using Sp converted phases. Pure Appl Geophys 2007;164:135–60. https://doi.org/10.1007/s00024-006-0158-3.

[50] Menke W. Geophysical data analysis: discrete inverse theoryVol. 322. Academic Press; 1989. ISBN0-12-490921-3.

[51] Menon R, Gerstoft P, Hodgkiss WS. On the apparent attenuation in the spatial coherence estimated from seismic arrays. J Geophys Res Solid Earth 2014;119:3115–32. https://doi.org/10.1002/2013JB010835.

[52] Menq FY. Dynamic properties of sandy and gravelly soils. Austin, Texas: Doctoral dissertation. University of Texas at Austin; 2003.

[53] Mucciarelli M, Gallipoli MR. Estimate of frequency and damping for large set of buildings in dense urban areas. In: First European conference on earthquake engineering and seismology, Geneva, Switzerland, September, 3–8; 2006.

[54] Nakahara H. Formulation of the spatial autocorrelation (SPAC) method in dissipative media. Geophys J Int 2012;190:1777–83. https://doi.org/10.1111/j.1365-246X.2012.05591.x.

[55] Ohori M, Nobata A, Wakamatsu K. A comparison of ESAC and FK methods of estimating phase velocity using arbitrarily shaped microtremor arrays. Bull Seismol Soc Am 2002;92:2323–32. https://doi.org/10.1785/0119980109.

[56] Okada H. The microtremor survey method. Translated by Koya Suto, Geophys Monogr., Vol. 12. Society of Exploration Geophysicists; 2003. https://doi.org/10.1190/1.9781560801740.

[57] Parolai S. Investigation of site response in urban areas by using earthquake data and seismic noise. In: Bormann P, editor. New manual of seismological observatory practice 2 (NMSOP-2); 2012. p. 1–38. Potsdam, Germany.

[58] Parolai S. Shear wave quality factor Q_S profiling using seismic noise data from microarrays. J Seismol 2014;18(3):695–704. https://doi.org/10.1007/s10950-014-9440-5.

[59] Parolai S, Bindi D, Ansal A, Kurtulus A, Strollo A, Zschau J. Determination of shallow S-wave attenuation by down-hole waveform deconvolution: a case study in Istanbul (Turkey). Geophys J Int 2010;181:1147–58. https://doi.org/10.1111/j.1365-246X.2010.04567.x.

[60] Parolai S, Mucciarelli M, Gallipoli MR, Richwalski SM, Strollo A. Comparison of empirical and numerical site responses at the Tito test site, southern Italy. Bull Seismol Soc Am 2007;97:1413–31. https://doi.org/10.1785/0120060223.

[61] Parolai S, Picozzi M, Richwalski SM, Milkereit C. Joint inversion of phase velocity dispersion and H/V ratio curves from seismic noise recordings using a genetic algorithm, considering higher modes. Geophys Res Lett 2005;32:L01303. https://doi.org/10.1029/2004GL021115.

[62] Picozzi M, Milkereit C, Parolai S, Jäckel KH, Veit I, Fischer J, Zschau J. GFZ wireless seismic array (GFZ-WISE), a wireless mesh network of seismic sensors: new perspectives for seismic noise array investigations and site monitoring. Sensors 2010;10(4):3280–304. https://doi.org/10.3390/s100403280.

[63] Pinna G, Poletto F, Corubolo P. Seismic attenuation analysis at OGS instrumented-well test site. In: Presentation, national group of solid earth Geophysics (GNGTS) 31st national conference, november 20th–22nd, Potenza; 2012.

[64] Poletto F, Petronio L, Farina B, Schleifer A. Seismic interferometry experiment in a shallow cased borehole using a seismic vibrator source. Geophys Prospect 2011;59:464–76. https://doi.org/10.1111/j.1365-2478.2010.00933.x.

[65] Prieto GA, Denolle M, Lawrence JF, Beroza GC. On amplitude information carried by the ambient seismic field. C R Geosci 2011;343:600–14. https://doi.org/10.1016/j.crte.2011.03.006.

[66] Prieto GA, Lawrence JF, Beroza GC. Anelastic earth structure from the coherency of the ambient seismic field. J Geophys Res 2009;114:B07303. https://doi.org/10.1029/2008JB006067.

[67] Riga E, Hollender F, Roumelioti Z, Bard PY, Pitilakis K. Assessing the applicability of deconvolution of borehole records for determining near-surface shear-wave attenuation. Bull Seismol Soc Am 2019;109(2):621–35. https://doi.org/10.1785/0120180298.

[68] Scherbaum F, Hinzen KG, Ohrnberger M. Determination of shallow shear wave velocity profiles in the Cologne, Germany area using ambient vibrations. Geophys J Int 2003;152:597–612. https://doi.org/10.1046/j.1365-246X.2003.01856.x.
[69] Sweeney DW, Vest CM. Reconstruction of three-dimensional refractive index fields from multidirectional interferometric data. Appl Opt 1973;12(11):2649–64. https://doi.org/10.1364/AO.12.002649.
[70] Tsai VC. Understanding the amplitudes of noise correlation measurements. J Geophys Res 2011;116:B09311. https://doi.org/10.1029/2011JB008483.
[71] Vasco DW. Extremal inversion of traveltime residuals. Bull Seismol Soc Am 1986; 76(5):1323–45.
[72] Vasco DW. Bounding seismic velocities using a tomographic method. Geophysics 1991;56(4):472–82. https://doi.org/10.1190/1.1443064.
[73] Wang Z, Street R, Woolery E. Q_S estimation for unconsolidated sediments using first arrival SH wave critical refractions. J Geophys Res 1994;99:13543–51. https://doi.org/10.1029/94JB00499.
[74] Warren N. Q and structure. The moon 1972;4:430–41. https://doi.org/10.1007/BF00562009.
[75] Wcisło M, Eisner L. Attenuation from microseismic datasets by the peak frequency method benchmarked with the spectral ratio method. Studia Geophys Geod 2016; 60:547–64. https://doi.org/10.1007/s11200-015-0577-7.
[76] Wcisło M, Stabile TA, Telesca L, Eisner L. Variations of attenuation and V_P/V_S ratio in the vicinity of wastewater injection: a case study of Costa Molina 2 well (High Agri Valley, Italy). Geophysics 2018;83:B25–31. https://doi.org/10.1190/geo2017-0123.1.
[77] Weemstra C, Boschi L, Goerts A, Artman B. Seismic attenuation from recordings of ambient noise. Geophysics 2013;78:1–14. https://doi.org/10.1190/geo2012-0132.1.
[78] Wessel P, Smith WHF, Scharroo R, Luis JF, Wobbe F. Generic mapping tools: improved version released. Eos Trans AGU 2013;94(45):409–10. https://doi.org/10.1002/2013EO450001.
[79] Wiggins RA. The general linear inverse problem: implication of surface waves and free oscillations for earth structure. Rev Geophys Space Phys 1972;10:251–85. https://doi.org/10.1029/RG010i001p00251.
[80] Xia J. Estimation of near-surface shear-wave velocities and quality factors using multichannel analysis of surface-wave methods. J Appl Geophys 2014;103:140–51. https://doi.org/10.1016/j.jappgeo.2014.01.016.
[81] Xia J, Miller RD, Park CB, Tian G. Determining Q of near-surface materials from Rayleigh waves. J Appl Geophys 2002;51:121–9. https://doi.org/10.1016/S0926-9851(02)00228-8.
[82] Yamanaka H, Ishida H. Application of generic algorithms to an inversion of surface-wave dispersion data. Bull Seismol Soc Am 1996;86:436–44.
[83] Yıldırım E, Saatçılar R, Ergintav S. Estimation of seismic quality factor. Artificial neural networks and current approaches. J Appl Geophys 2017;136:269–78. https://doi.org/10.1016/j.jappgeo.2016.11.010.
[84] Zelt CA, Barton PJ. Three-dimensional seismic refraction tomography: a comparison of two methods applied to data from the Faeroe Basin. J Geophys Res Solid Earth 1998;103(B4):7187–210. https://doi.org/10.1029/97JB03536.
[85] Zhang C, Ulrych TJ. Estimation of quality factors from CMP records. Geophysics 2002;67(5):1542–7. https://doi.org/10.1190/1.1512799.